Effect of shock compression method on the defect substructure in monocrystalline copper[☆]

Bu Yang Cao [a], David H. Lassila [b], Matt S. Schneider [a], Bimal K. Kad [a], Chong Xiang Huang [c], Yong Bo Xu [c], Daniel H. Kalantar [b], Bruce A. Remington [b], Marc Andre Meyers [a],*

[a] *Materials Science and Engineering Program, University of California, San Diego, 9500 Gilman Dr., UCSD 0411, La Jolla, CA 92093, USA*
[b] *Lawrence Livermore National Laboratory, Livermore, CA 94550, USA*
[c] *Chinese Academy of Sciences, Shenyang Natl. Lab. for Matls. Sci., Inst. of Metal, Shenyang, Liao Ning 110016, China*

Abstract

Monocrystalline copper samples with orientations of [0 0 1] and [2 2 1] were shocked at pressures ranging from 20 to 60 GPa using two techniques: direct drive lasers and explosively driven flyer plates. The pulse duration for these techniques differed substantially: 40 ns for the laser experiments at 0.5 mm into the sample and 1.1∼1.4 µs for the flyer-plate experiments at 5 mm into the sample. The residual microstructures were dependent on orientation, pressure, and shocking method. The much shorter pulse duration in the laser driven shock yielded microstructures in recovery samples closer to those generated at the shock front. For the flyer-plate experiments, the longer pulse duration allows shock-generated defects to reorganize into lower energy configurations. Calculations show that the post-shock cooling for the laser driven shock is $10^3 \sim 10^4$ faster than that for plate-impact shock, increasing the amount of annealing and recrystallization in recovery samples for the latter. At the higher pressure level, extensive recrystallization was observed in the plate-impact samples, while it was absent in laser driven shock. An effect that is proposed to contribute significantly to the formation of recrystallized regions is the existence of micro-shear-bands, which increase the local temperature beyond the prediction from adiabatic compression.
© 2005 Elsevier B.V. All rights reserved.

Keywords: Laser; Shock compression; Plate impact; Shear localization in copper; Shock waves; Explosives

1. Introduction

It is indeed a distinct honor to give a presentation in this symposium and to author a paper commemorating this festive occasion. The principal themes of Prof. J.C.M. Li's work have been micromechanisms of mechanical behavior in crystalline and amorphous materials (metals, metallic glasses, porous materials, and polymers). The nature of his work has been both theoretical and experimental. Professor Li is undoubtedly one of the global authorities in this field, and his contributions have spanned 50 years. Among the numerous original inroads into heretofore uncharted territory, the following come to mind:

- mechanism for plastic deformation of metallic glasses (e.g. [1–4]);
- shear localization in metallic glasses (e.g. [2–4]);
- mechanism for the grain-size dependence of yield stress (e.g. [5]);
- use of impression testing using micron-sized cylindrical indenters to determine adhesion, creep resistance, viscosity, and the kinetics of stress relaxation (e.g. [6]);
- dislocation dynamics through stress relaxation (e.g. [6,7]);
- combustion synthesis of intermetallic compounds (e.g. [8]);
- thermally-activated description of plastic flow (e.g. [9]).

Shock compressed materials show a great variety of microstructures in which the mechanisms envisioned by Prof. Li play a pivotal role. Although the effects of the uniaxial-strain high-strain-rate loading have been studied for the past 50 years, not all aspects have been elucidated. Smith [10] first described the shock compression of materials in mechanistic terms. In the early techniques, samples were subjected to shock compression

by explosives, either by direct loading or by impact. The samples were recovered and the microstructure was analyzed to evaluate the effects of the shock pre-straining on the material. Later, different kinds of experiments have been designed to investigate the dynamic behavior of different materials [11–15].

Recovery experiments provide a convenient way to study defect generation and energy storage mechanisms in materials subjected to shock waves especially given the difficulty involved in studying the physical properties of the materials during the shock (rapid loading rate and short time interval). Since that time, much work has been done on quite a number of materials to develop a hydrodynamic understanding of the material behavior, and several reviews have summarized the systematic changes in the structure–property relationships generated by shock wave passage through the material [16,17]. Most of this work correlates the microstructure and mechanical property changes to the compression characteristics like peak pressure, pulse duration, rarefaction rate, and even temperature. Also, much work has been done to model these responses and to compare the behaviors to those observed at low strain rates [16–18]. Remington et al. [19] review the most significant recent work.

For the experimental techniques of shock compression, it is essential that the principal parameters be well characterized in the experiments. Flyer-plate impact and laser shock are two typical loading methods employed in shock–recovery experiments. In the flyer-plate impact experiment, the plate impacts a target at a known velocity. If the impact is perfectly planar and if the velocity vector of the impacting plate is perfectly normal to the impact plane, then a state of pure one-dimensional strain will be produced in both flyer plate and target. The minimization of lateral strain in shock compression has been shown by Gray et al. [20] and Mogilevsky and Teplyakova [21] to be important.

Lasers deliver high energy densities in extremely short pulse durations enabling research in regimes of pressure and strain rates never before explored. Lasers have been shown to generate pressures from 10 to over 500 GPa. The TPa regime is also currently accessible (e.g. [22]) through the use of the *hohlraum* concept. R. Cauble et al. developed methods to obtain the equation-of-state data in the 10–40 Mbar (1–4 TPa) regime [23]. Lasers also provide an easy way to vary pulse duration ("dwell time") with picosecond resolution, which can then be correlated to the pressure data to yield a strain rate. Lasers typically produce less residual strain as compared to other techniques and post-shock heating is minimized because of the short-duration pulses and the small specimen size/geometry. Laser-driven shocks are created by the rapid heating of the surface from the intense laser illumination of the material [24]. Lasers are uncovering a new frontier in materials dynamics under extreme states of shock compression.

Both the flyer-plate impact [25] and laser [26] techniques have recently been employed to explore the post-shocked residual microstructures of monocrystalline copper. Significant differences in the residual microstructure have been observed at high pressures.

It is the objective of this paper to demonstrate that the differences of the residual microstructures (which are orientation dependent) are to a large extent due to how the heat gener-

ated inside the samples during shock is extracted. Post-shock recovery (annealing) and recrystallization processes dominate the residual microstructures, if the time interval and temperature are sufficient. The unique advantage of laser shock compression over plate impact, namely the rapid post-shock cooling, is discussed.

2. Experimental methods

Explosively driven flyer plates and direct drive lasers produce different shock pulses. Fig. 1 shows the characteristic shapes of these two shock waves. The shock wave produced by plate impact has initially a square shape (Fig. 1(a)) [24]. It has a flat top that has a length equal to twice the time required for the wave to travel through the projectile. The portion of the wave in which the pressure returns to zero is called the "release". During impact, elastic waves with velocity C_0 and shock waves with velocity U_s are emitted into the target and projectile. For the experiments reported herein, the duration of the pulse at a depth of 5 mm from the impact interface was in the 1.1–1.4 μs range. For the cases studied here (thick samples, ∼1 mm) and moderately short laser pulses (2–3 ns), the launched shock quickly
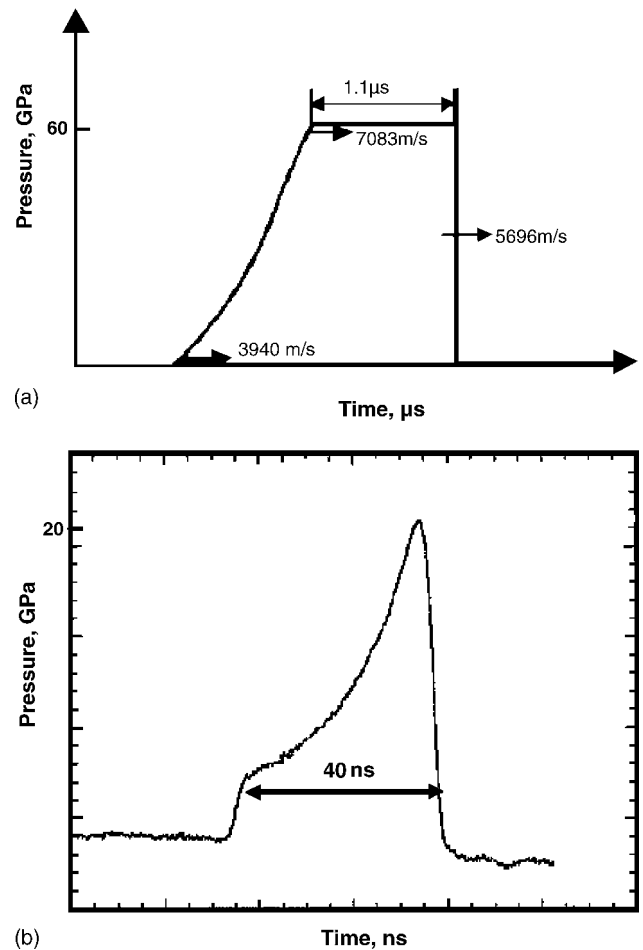

Fig. 1. Shock wave configurations: (a) shock wave (trapezoidal) produced by plate impact: time duration is 1.1 μs and peak pressure is 60 GPa; (b) pulse shape of typical laser shock experiment: time duration is 40 ns and peak pressure to 20 GPa.
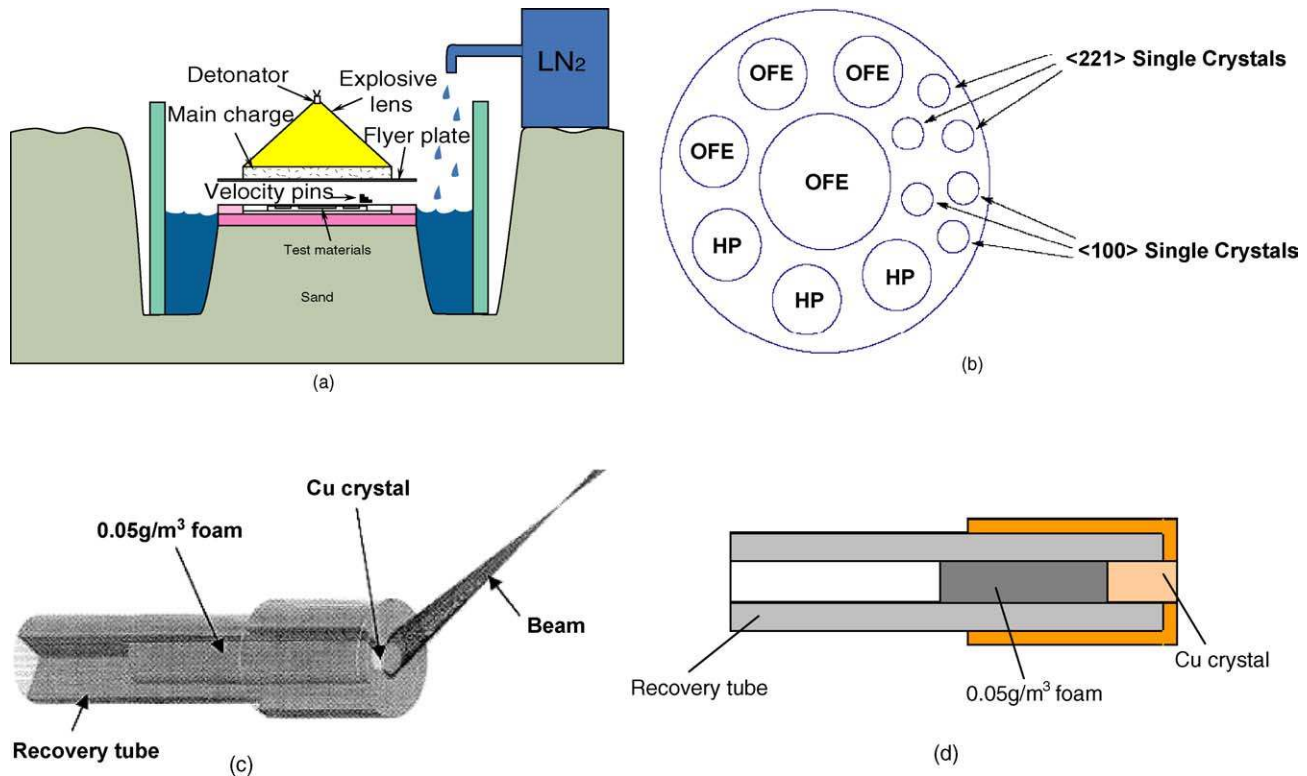
Fig. 2. The experimental sets for two kinds of shock compression methods: (a) shock–recovery experiments performed by acceleration of a flyer plate by an explosive charge; (b) anvil with OFE, HP and single crystal test samples; (c) sample and recovery chamber for laser shock experiments; (d) the cross section of the samples and recovery chamber for laser shock experiments.

evolves into a blast wave, which has a triangular shape. A typical pulse shape is shown in Fig. 1(b). At 0.5 mm into the sample, the pulse duration is around 40 ns, at an energy around 300 J, at a laser energy of around 300 J, which produces an initial pressure of approximately 60 GPa. In our experiments, phase plates were also utilized to smooth the beam over the entire surface of interest. Thus, the difference in the sample pressure duration (pressure dwell time) is of order ∼1000.

In the explosion-driven flyer-plate experiments, two orientations of monocrystalline copper, $\langle 0\,0\,1 \rangle$ and $\langle 2\,2\,1 \rangle$ were shock-compressed in the shock/recovery experiments at low temperature (88 K). The setup used for this experiment is shown in Fig. 2(a). It is described in detail by Lassila et al. [25]. The copper samples were shocked by an explosion-driven flyer plate, providing an initial pulse duration of 1.4 μs for a 30 GPa and 1.1 μs for a 60 GPa shock. The monocrystalline cylinders, with a diameter of 20 mm and thickness of 4.5 mm, were embedded in a copper plate (Fig. 2(b)). Lateral and bottom momentum traps were employed to trap the lateral release waves and to prevent spalling of the copper. These traps were made from a Cu–Be alloy because of its enhanced strength relative to unalloyed Cu. The flyer-plate velocity was determined by using pins located in four positions equally spaced around the lateral momentum trap (Fig. 2(a)). The shock pressures were determined using the flyer-plate velocity in conjunction with the U_s versus U_p linear relationship. The copper samples were shocked at 30 and 57 GPa, from an initial temperature of 88 K obtained by cooling the assembly with liquid nitrogen. The surface of the monocrys-

tals was protected from direct impact by electrodeposition of Cu cover plate material, followed by finish machining to a high tolerance (prior to electrodeposition, the Cu samples were protected with a release agent).

The laser shock experiments were primarily carried out at the OMEGA Laser Facility at University of Rochester's Laboratory for Laser Energetics (LLE). Preliminary and follow-up experiments were performed using the JANUS Laser at Lawrence Livermore National Laboratory (LLNL). The input laser energies used in the experiments were, for [0 0 1]: 40 J, 70 J, 205 J, and 300 J. For the [2 2 1] orientation, one experiment at laser energy of 300 J was carried out. The energies can be translated into pressures using Lindl's equation [27]:

$$P = 40 \left(\frac{I_{15}}{\lambda} \right)^{2/3} \tag{1}$$

where P is pressure (MBar), I_{15} the laser intensity (10^{15} W/cm^2), and λ is wavelength in micrometers. The laser spot size was on the order of 2.5–3 mm, depending on the size of the sample and the pulse durations were typically 2.5 ns with a small number of experiments occurring at 6 ns. This experimental setup provided energy densities on the order of 50 MJ/m^2. For the recovery experiments, single crystals of Cu with an [1 0 0] orientation were obtained from Goodfellow in the form of disks with 2.0–3.0 mm diameter and 1 mm thickness. They were mounted into foam-filled recovery tubes shown in Fig. 2(c). Foam with a density of 50 mg/cm^3 was used to decelerate the samples for

recovery. The shock amplitude at the surface of the Cu crystal can be obtained from the laser energy and the computed values (using hydrocode calculations). In some experiments, a CH plastic layer was used as an ablator. This resulted in an impedance mismatch at the CH/Cu interface, which enhanced the shock pressure in the copper specimen. Due to the short duration of the shock created by the 3 ns laser pulse, the decay in the specimen is very rapid. This decay is calculated by a hydrodynamics code.

3. Experimental results

3.1. Deformation microstructures for plate impact and laser shock at 30–40 GPa

The microstructures are characterized by stacking faults for both the plate impacted and laser shocked ⟨1 0 0⟩ samples, as shown in Fig. 3. This is known and has been established by Murr [28,29], among others. The average spacing between stacking faults is between 230 and 450 nm for the laser shocked samples and between 180 and 220 for the plate-impact shocked sample. Fig. 3(a and b) show the stacking-fault patterns similar to the ones observed by Murr [30] for the 30 GPa plate-impact shocked samples. It shows the two sets of stacking faults as the traces of [$\bar{2}$ 2 0] and [2 2 0] orientations in the (0 0 1) plane when the TEM electron beam direction is $B = \langle 0\,0\,1\rangle$. Fig. 3(c) shows the stacking faults formed in 40 GPa laser shocked samples. All four stacking-fault variants, viz. the (1 1 $\bar{1}$)1/6[1 1 2], (1 1 1)1/6[$\bar{1}$ $\bar{1}$ 2], ($\bar{1}$ 1 1)1/6[1 $\bar{1}$ 2], and (1 1 $\bar{1}$)1/6[$\bar{1}$ $\bar{1}$ 2] are observed, indicated as A, B, C, and D. This is due to the fact that, for [0 0 1], they all have the same resolved shear stress. However, there is a significant difference in the activation along [$\bar{2}$ 2 0] (SF: A, B) versus [2 2 0] (SF: C, D) with the density of occurrence significantly higher in the former. It should be noted that, in the 30 GPa plate-impact shocked ⟨1 0 0⟩ monocrystalline copper samples, we observed isolated regions of recrystallization as well as localized deformation bands. These were absent for the laser shocked specimens.

The substructure of the plate impacted ⟨2 2 1⟩ sample shocked at 30 GPa contains bands, whose morphologies vary through this sample. Some large bands, shown in the left part of Fig. 4(a), have a width around 120–130 nm. Micro-bands with a width of 20–30 nm were found within these large bands. More detailed TEM shows that there are two sets of micro-bands with an angle of around 70°; one direction is more predominant than the other one. Huang and Gray [31] proposed a model to explain the formation of micro-bands, based on the development of coarse slip bands. In their model, double dislocation walls are formed parallel to the primary slip planes at first. Secondary slip is induced by the internal stresses in the region between the double walls. Then, the interaction of the primary and secondary dislocations results in a final stable dislocation configuration. The laser shocked ⟨2 2 1⟩ samples are characterized by a greater density of twins than bands. Although some bands with width of 100–200 nm were observed, very similar to those big bands in the 30 GPa plate impacted samples, twins were more prevalent throughout the sample. Fig. 4(b) shows two traces of twins with a (1 $\bar{1}$ 1) habit plane.
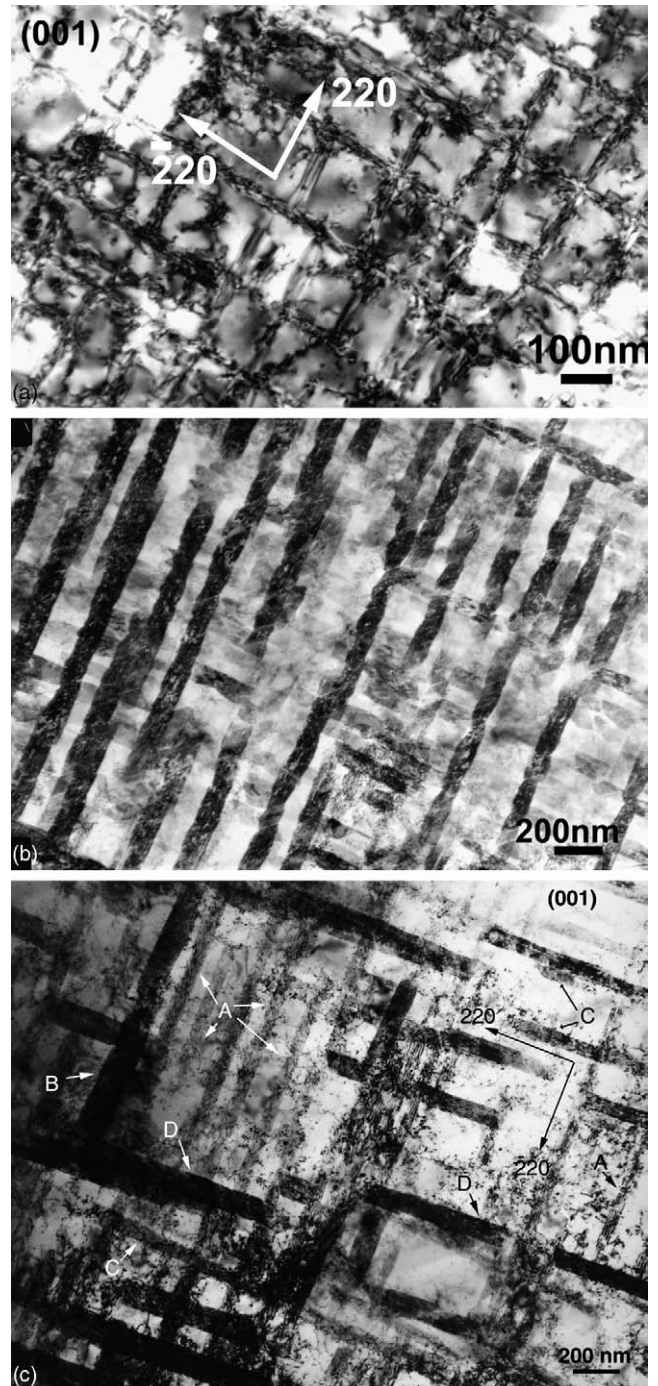

Fig. 3. (a) Stacking faults in 30 GPa plate-impacted ⟨1 0 0⟩ sample; (b) stacking faults in 30 GPa plate-impacted ⟨1 0 0⟩ sample with large magnification; (c) 40 GPa laser shocked ⟨1 0 0⟩ sample (from Meyers et al. [25]): four sets (marked as A, B, C, D) are observed. Variant A exhibits the highest density of occurrence. Energy input = 205 J, g = 200, B = [0 0 1].

3.2. Deformation microstructures for plate impact and laser shock at 55–60 GPa

Micro-twins occur in the samples shocked at 55–60 GPa both in the plate impact and the laser shock cases. In plate-impacted ⟨1 0 0⟩ monocrystalline samples, as shown in Fig. 5(a), there is only one set of micro-twins with ($\bar{1}$ $\bar{1}$ 1) as their habit plane. The
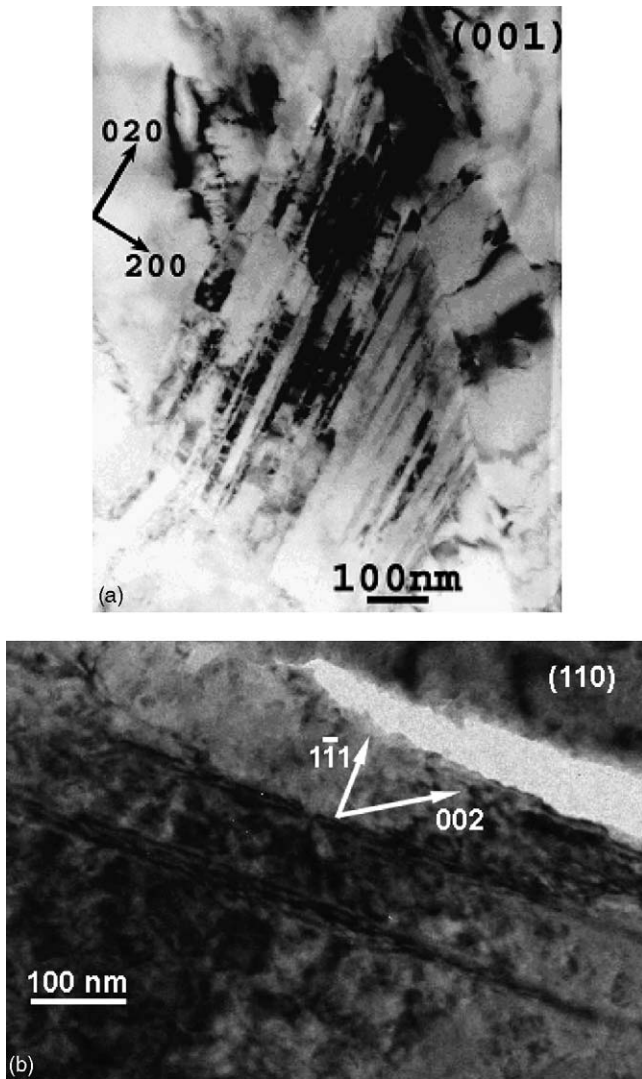
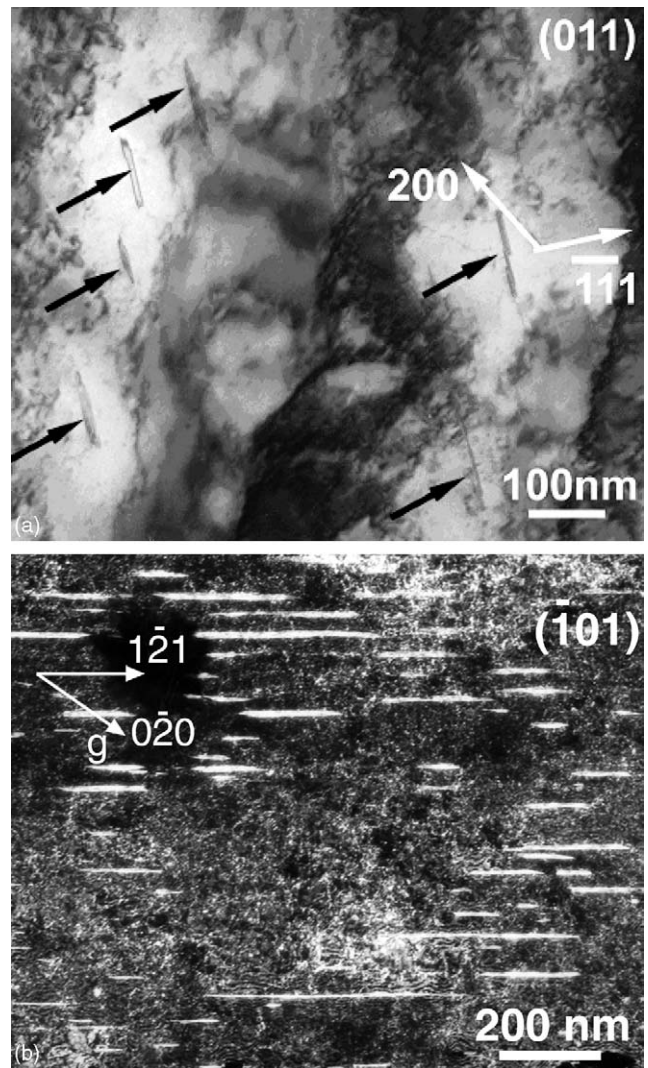Fig. 4. (a) Micro-bands in 30 GPa plate-impacted ⟨2 2 1⟩ samples; (b) twins in 35 GPa laser shocked ⟨2 2 1⟩ samples.

Fig. 5. (a) 57 GPa plate-impacted sample: micro-twins with the habit plane of (1 1̄ 1) shown at the electron beam direction of (0 1 1); (b) 55–60 GPa laser shocked sample (from Meyers et al. [25]): micro-twins with a (1 1 1) habit plane elongated along [1 2̄ 1] in 60 GPa laser shocked ⟨1 0 0⟩ sample. Energy input = 320 J, $g = 0$–20, $B = [1\,0\,1]$.

sizes for the micro-twins vary from 80 to 180 nm. For the laser-shocked ⟨1 0 0⟩ samples, there are two sets of micro-twins. When imaged at $B = [0\,0\,1]$, they appear at exactly 90 degrees to each other aligned along [2 2 0] (set A) and [2̄ 2 0] (set B) directions, respectively, and they are present roughly in the same proportion (not shown here). Set A exhibits a wide range of lengths, from as small as 70 nm to as large as 1 μm; the mean value is around 125 nm. In contrast, the set B micro-twins have a near uniform length of 70 nm. Fig. 5(b) shows set A, which has the (1 1 1) habit plane and are elongated along [1 2̄ 1], when imaged in the edge orientation at B close to [1̄ 0 1]. It should be noted that the deformation microstructure was not uniform around the perforation in either of the two kinds of samples.

For the 57 GPa plate-impact shocked samples, there are deformation bands, slip bands, recrystallized regions and dislocation tangles in addition to micro-twins. Fig. 6(a) shows an overview TEM near the back surface of the specimen. A deformation band with approximately 1.8 μm width is seen traversing the specimen. In comparison with the slip/stacking-faults bands around it,

this deformation band is larger and breaks them up. Selected area diffraction identifies the vertical slip bands as (1 1̄ 1). It appears that the horizontal slip bands were activated earlier than the vertical bands because the horizontal bands seem to be interrupted by the vertical ones. One can also see that the appearance of these stacking faults is different from the ones shown in Fig. 3. There is evidence for recovery processes within them. These broad bands are absent in the laser shock case because of the much shorter time intervals involved. Indeed, the shock velocity is approximately 5.6 mm/μs. A duration of 1.4 μs can generate heterogeneities extending over a few millimeters. On the other hand, for the laser shock case, with a duration of 40 ns at 0.5 mm, the ability to generate inhomogeneities is much more restricted. These would be a few micrometers long, and their thickness would be greatly reduced. In Fig. 6(b), for the plate impact case, regular dislocation cell arrays can be seen. Between two arrays, there are dislocation tangles and in some places the density of
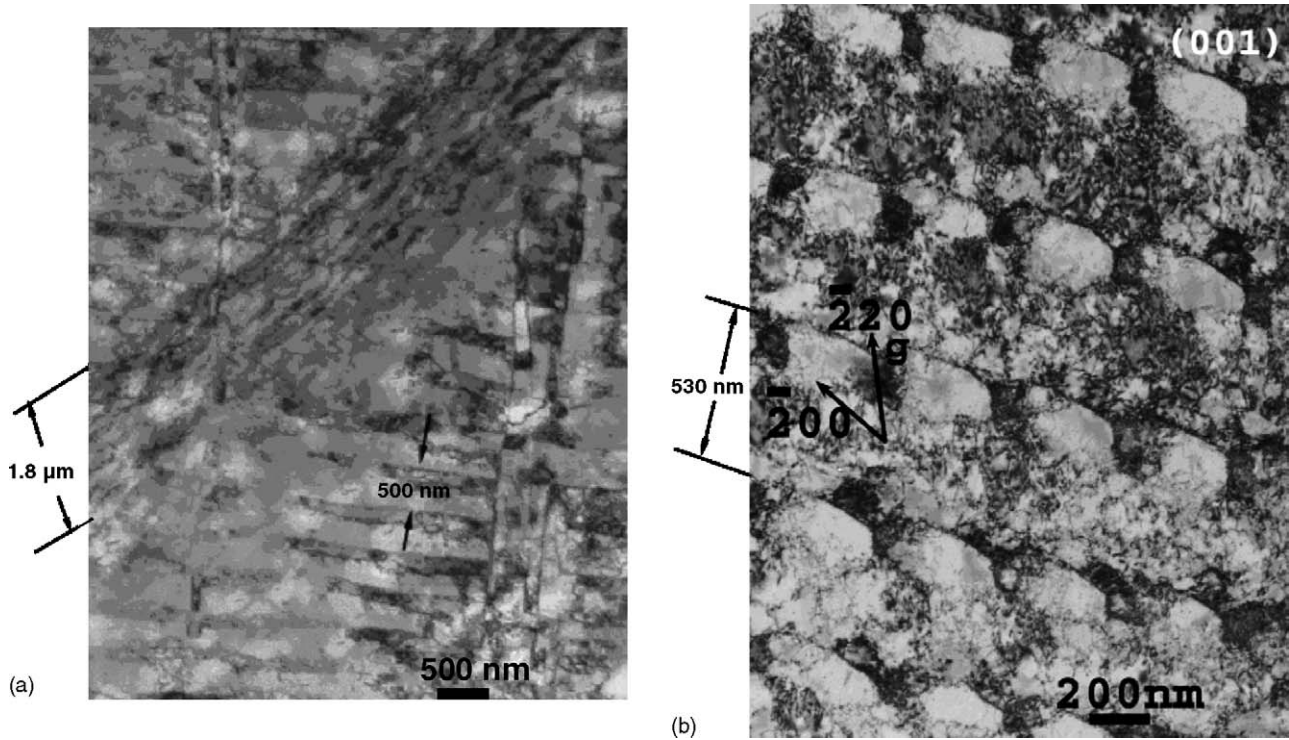
Fig. 6. TEM for 57 GPa plate-impacted ⟨1 0 0⟩ copper samples: (a) overview of the sample (×10 K); (b) dislocation circles shown in the first thin foil along the shock direction.

dislocation is very high. By comparing the TEM observations in different positions, the dislocation density becomes lower along the shock direction. Extended regions of dislocation arrays and stacking faults can be seen. By measuring the distances between the repeated structures in both Fig. 6(a and b), as indicated in the two pictures, it can be seen that the two different structures have the same width of around 500 nm. The periodicity of the features of Fig. 6(a) is remarkable. It is speculated that these features are due to the recovered stacking-fault arrays seen in Fig. 6(b). Mughrabi and Ungar [32] found some dislocation cell structures very similar to our observations, but they are quite unlike the cells observed by other investigators (e.g., Johari and Thomas [33]). Gray and Follansbee [34] believe that increasing peak pressure or pulse duration decreases the observed dislocation cell size and increases the yield strength.

However, the major difference between the laser shocked samples and plate-impact shocked samples in 55–60 GPa regime is the presence of fully recrystallized regions in the latter. The recrystallized grains in the 57 GPa plate-impact shocked ⟨1 0 0⟩ sample are similar to those for the 30 GPa plate impact, but much more extensive.

For the 55–60 GPa laser shocked samples, there are some laths away from the center (Fig. 7), while micro-twins are situated closer to the center. Unlike the micro-twins, the laths are elongated close to ⟨2 2 0⟩. In some regions they are aligned along [$\bar{2}$ 2 0] and in others along [2 2 0]. The intermediate area shows laths misoriented from [2 2 0]. Given the curvature of the laths, it is unlikely that they conform to any single habit plane. Nonetheless, the projected width of the lath interface shows a minimum at $B = $ [0 0 1], and a maximum at either [1 0 1], or [$\bar{1}$ 0 1], where the respective {1 1 1} are in the edge orientation. The lath inter-

face plane is parallel to [0 0 1], and therefore, uniquely different from micro-twins. In fact, on rare occasions we observe laths containing some micro-twins.

Meyers [26] explained the features revealed in Fig. 7 for laser shocked samples. These features are believed to be consistent with the "wavy sub-grains" observed after high-pressure shock compression by Murr [30] (in particular, note the similarities with Figs. 34 and 35 in ref. [30]). This structure is also analogous to the one observed by Gray [35] in specimens where the residual strain was high. Thus, it is suggested that the substructures are due to thermal recovery of the shock-induced microstructure.
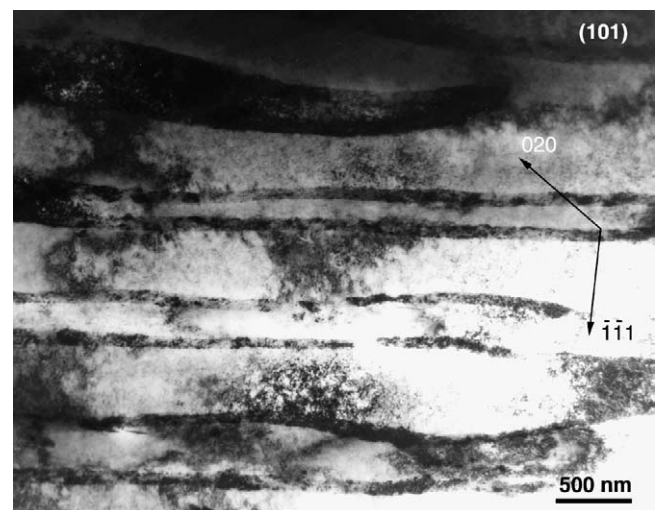

Fig. 7. View of laths imaged at beam direction $B = $ [1 0 1] in 55–60 GPa laser shocked ⟨1 0 0⟩ samples (from Meyers et al. [25]).

The orientation close to $\{1\,1\,1\}$ of the boundaries is a residue of the original twin boundaries. This microstructure represents the recovered state of a heavily twinned and dislocated structure. While for the plate-impact shocked samples at the same pressure, the heavily dislocated structures may indicate that the there is not as much as thermal recovery in the laser shocked samples.

The $\langle 2\,2\,1 \rangle$ samples plate-impacted at 57 GPa were full of large recrystallized grains, which were shown by both TEM and SEM – Electron Channeling Contrast [36] in Fig. 8(a and b). Annealing twins grow in the recrystallized grains. In 60 GPa laser shocked $\langle 2\,2\,1 \rangle$ samples, there is a high density of dislocation, as shown in Fig. 9(a). These dislocations are tangled and some bands were formed as a result of heavy dislocation density. Deformation twins were found in this sample, as shown in Fig. 9(b).

4. Analysis

4.1. Heat extraction from shocked specimens

Laser and plate-impact shocks have different wave shapes and very different duration times: 2 ns for the laser experiments and 1–2 μs for flyer-plate experiments. It is important to note these here because this likely results in very different effects on the heat generated during the shock and the heat transfer afterwards.

When a shock wave compressed the sample, the shock amplitude attenuates along the propagation direction. We can see from Fig. 1(a) that the rarefaction overtaking the peak pressure plateau from the back travels with the velocity of $C + U_p$. The front of the shock wave travels with the velocity of U_s. The bottom of the part that is beyond the peak pressure travels with a velocity of C_0. Hence, eventually the rarefaction will catch up with the shock front, leading to a triangular shaped blast wave, much like in the laser experiment. For the plate-impact shock wave, the distance that the peak pressure is maintained, S, can be calculated to a first approximation by:

$$S = \frac{U_s^2 t_p}{U_p + C - U_s} \tag{2}$$

$$U_s = C_0 + S_1 U_p \tag{3}$$

This calculation in Eq. (2) neglects the advance of the interface. If we do consider that, a more precise solution is given as Eq. (4):

$$S = \frac{U_s C t_p}{U_p + C - U_s} \tag{4}$$

The parameters for copper are: $S_1 = 1.489$; when $P = 60$ GPa, $U_{s1} = 5.696$ km/s, $U_{p1} = 1.180$ km/s, $C_1 = 5.903$ km/s; when $P = 30$ GPa, $U_{s1} = 4.95$ km/s, $U_{p1} = 0.679$ km/s, $C_1 = 5.131$ km/s. Thus, when the peak pressure is 60 GPa, the distance that the peak pressure is maintained, S, will be 25.73 mm and 26.67 mm, according to Eqs. (2) and (4), individually.

We can, thus, obtain the progress of the shock pulse through the sample and its decay, shown in Fig. 10(a) for both 30 and 57 GPa. Fig. 10(b) represents the shock pressure decay for laser shocked samples, extracted from the laser impact energies and
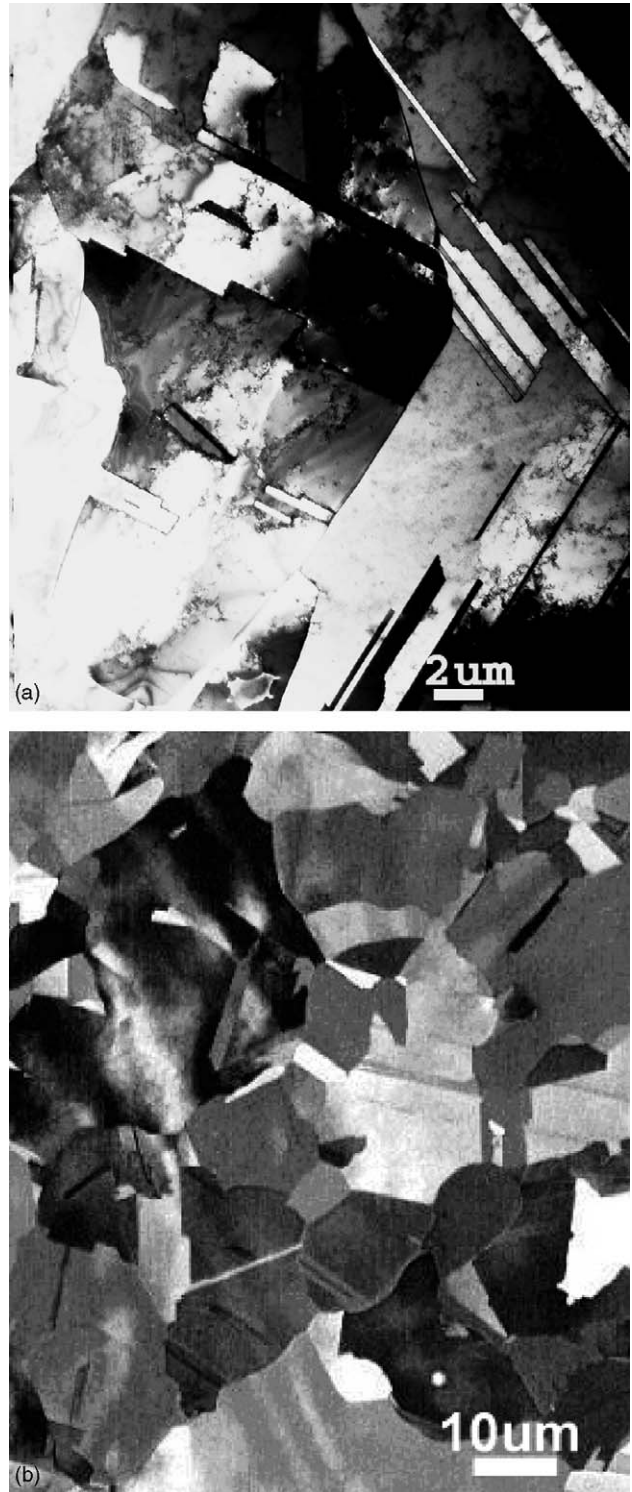

Fig. 8. 57 GPa plate-impacted $\langle 2\,2\,1 \rangle$ sample (a) TEM showing annealing twins and recrystallized grains in; (b) recrystallized grains were observed by SEM–ECC in 57 GPa impacted $\langle 2\,2\,1 \rangle$ sample.

hydrocode calculations. Note that the maximum pressure versus distance plotted in Fig. 10(b), at small distances, is nearly the same as the laser ablation pressure (Eq. (1)), which can be high, at the higher laser energies. There is an exponential decrease as a function of propagation distance. The difference between the
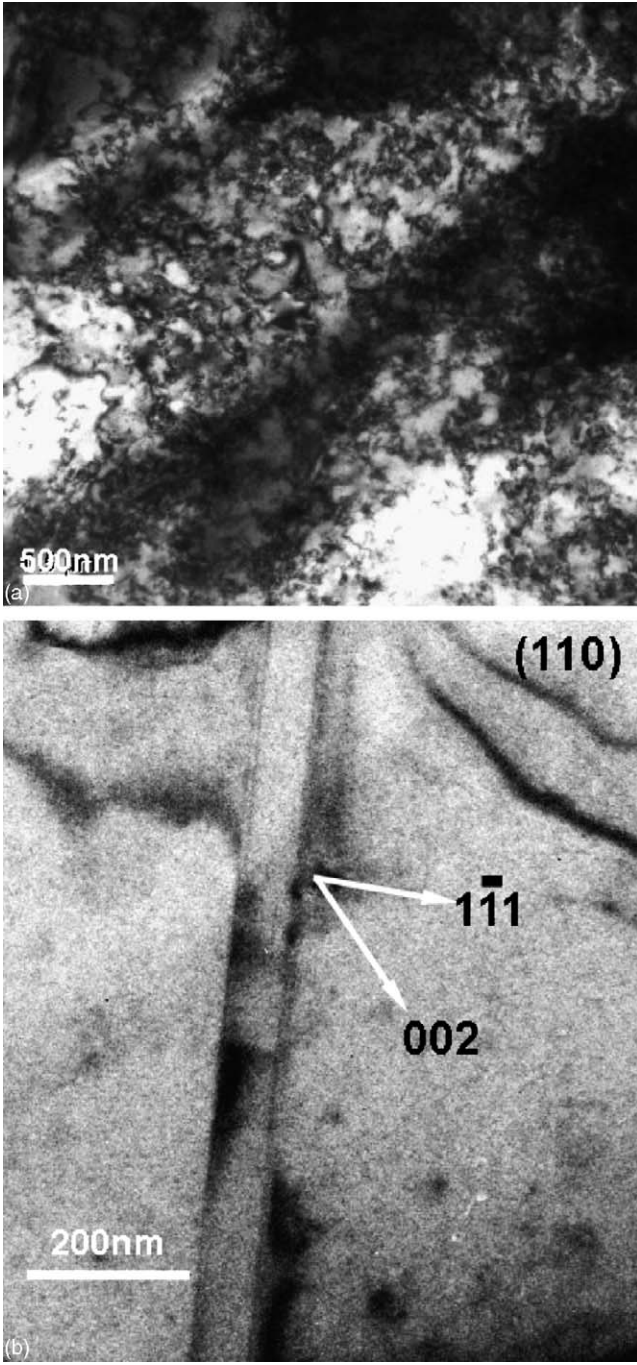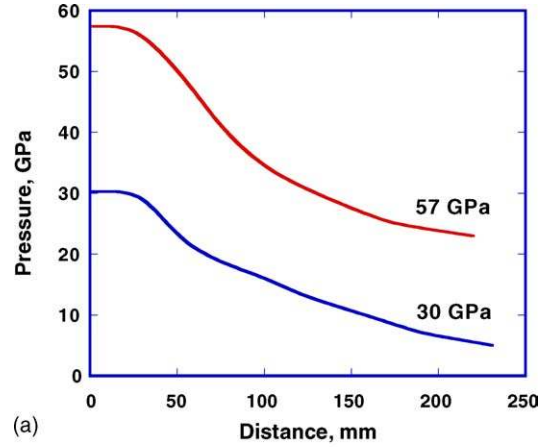
Fig. 9. 60 GPa laser shocked ⟨2 2 1⟩ samples: (a) dislocation structures; (b) twins.

Fig. 10. Pressure profiles along the samples during shock: (a) plate-impact shock; (b) laser shock from Meyers et al. [26].
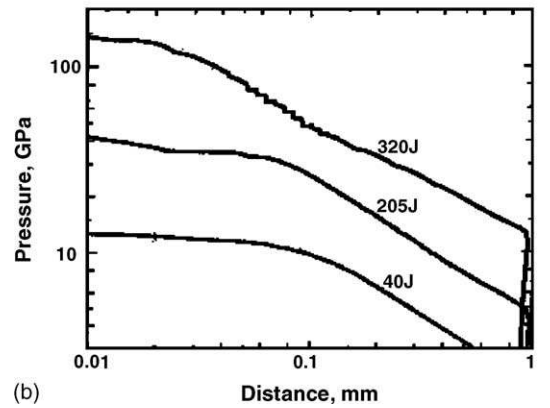
decay rates in Fig. 10(a and b) is the result of the difference in pulse duration.

Based on the pressures given in Fig. 10, the shock and residual temperatures inside the samples can be calculated through Eqs. (5) and (6) [17]. The shock temperature T_s is:

$$T_s = T_0 \exp\left[\frac{\gamma_0}{V_0}(V_0 - V_1)\right] + \frac{P(V_0 - V_1)}{2C_v} + \frac{\exp\left[\frac{-\gamma_0}{V_0}V_1\right]}{2C_v}$$

$$\times \int_{V_0}^{V_1} P \exp\left(\frac{\gamma_0}{V_0}V\right)\left[2 - \frac{\gamma_0}{V_0}(V_0 - V)\right] dV \quad (5)$$

The residual temperature T_r is:

$$T_r = T_s \exp\left[\frac{-\gamma_0}{V_0}(V_0 - V_1)\right] \quad (6)$$

γ_0 is 1.99 for copper, P the peak pressure of the shock waves, V_1 is the specific volume of the material directly behind the shock; V_1 can be calculated from the relationships between the shock parameters.

$$P = \frac{C_0^2(V_0 - V)}{[V_0 - S(V_0 - V)]^2} \quad (7)$$

$$V = \frac{C_0^2}{2PS^2}\left[\sqrt{1 + \frac{4PSV_0}{C_0^2} + \frac{2S(S-1)V_0P}{C_0^2}} - 1\right] \quad (\text{m}^3/\text{kg}) \quad (8)$$

C_0 and S are the parameters used to describe the relationship between shock velocity U_s and particle velocity U_p:

$$U = C_0 + S_1 U_p + S_2 U_p^2 + \cdots \quad (9)$$

For Cu, $C_0 = 3.94 \times 10^3$ m/s, $S_1 = 1.489 \times 10^3$ m/s. We also need to consider the heat capacity C_v (the specific heat at constant volume). The values of specific heat at constant pressure

C_p usually are easier to measure than C_v. C_v can be evaluated solely from C_p and P versus T data.

$$C_v = T\left(\frac{\partial S}{\partial T}\right)_v \tag{10}$$

$$C_p = T\left(\frac{\partial S}{\partial T}\right)_p \tag{11}$$

$$C_p - C_v = \frac{vT\beta^2}{K_T} \tag{12}$$

where v is the specific volume, β is the volumetric expansion coefficient and K_T is the isothermal coefficient of compressibility.

Using Eqs. (2)–(11), the residual temperatures throughout the samples immediately after shocking (no heat transfer) can be calculated. The calculated values are shown in Fig. 11. The initial temperature, T_0, at which the samples were shocked, is 88 K for plate impact, and 298 K for laser shock.

The second step is to calculate the heat transfer after the shock. The following assumptions are made: (1) heat conduction is one-dimensional; (2) the copper sample is a semi-infinite medium; (3) copper sample has uniform and constant thermal properties; (4) temperature profiles at time $t = 0$ are shown in Fig. 11 (no interaction between the traveling wave and heat transfer). Assumption 4 is justified by the fact that the ther-

(a)

(b)

Fig. 11. Residual temperature inside the sample immediately after shock: (a) plate-impact shock; (b) laser shock.

mal transport velocity is negligible in comparison with the wave propagation velocity when shock pressure is less than 100 GPa.

Rate of heat conduction into control volume = Rate of heat conduction out of control volume + Rate of energy storage inside control volume

Dividing the samples into small elements of $N - 1$ pieces ($1 < i < N$) and Δx is the discrete spatial step, and defining a discrete time step Δt analogous to Δx.

$$t_m = m\Delta t \quad (m = 0, 1, ...) \tag{13}$$

Calculate the heat transfer separately [37]:

$$T_{i,m+1} = T_{i,m} + \frac{\Delta t k}{\rho c \Delta^2 x}(T_{i+1,m} - 2T_{i.m} + T_{i-1,m})$$
$$\text{for } (1 \leq i \leq N) \tag{14}$$

Consider specified flux boundary conditions as:

$$T_{1,\text{new}} = T_{1,\text{old}} + (T_{2,\text{new}} - T_{1,m})$$
$$T_{N,\text{new}} = T_{N,\text{old}} + (T_{N-1,\text{new}} - T_{N,m}) \tag{15}$$

For copper, the parameters are: K (thermal conductivity) equals to 401 W/(m K); C (specific heat), $C_{300\,K} = 364$ J/(kg K); ρ (density), $\rho_{300\,K} = 8920$ kg/m^3; D (thermal diffusivity), $D = \frac{k}{\rho C_p}$.

Figs. 12 and 13 show the change of temperature with time, $T(t) - T_0$, for 30 and 57 GPa plate impacts. For 30 GPa, the maximum temperature (at surface) changes from approximately 160–100 K during a period of 1000 s. For 57 GPa, the maximum temperature changes from approximately 360 to 140 K during this same time period (1000 s). This period of time should be sufficient to induce some microstructural changes inside the samples. Fig. 14 shows the temperature changes at a fixed section for a distance $L = 5$ mm from the impact interface. One can see that in the front part of the sample (within 5 mm), the temperature remains above 160 K (for the 57 GPa shock), and above 100 K (for the 30 GPa shock) for 1000 s.

For the laser shock case, the region which is affected by the temperature rise is much shorter (up to 1mm, as shown in Fig. 11). The temperature excursions in laser shocked samples are shown in Figs. 15 and 16. These results were calculated by the same procedure as the plate-impact samples (Figs. 12 and 13). By comparing the temperature changes in those two experiments, it is easy to notice that, first, the laser shock affected distance is much shorter and second, the temperature drop is much more rapid for laser shock.

Based on these analyses, a qualitative comparison of the plate impact and laser shock can be estimated. The temperature decays in the laser shocked sample are $10^3 \sim 10^4$ faster than those in the plate-impacted sample. These results explain why, although the peak pressures of laser shock are much higher than those of impact (Fig. 10), resulting in higher residual temperatures (Fig. 11), the post-shock microstructures in plate impact samples show a greater effect of post shock thermal excursion.
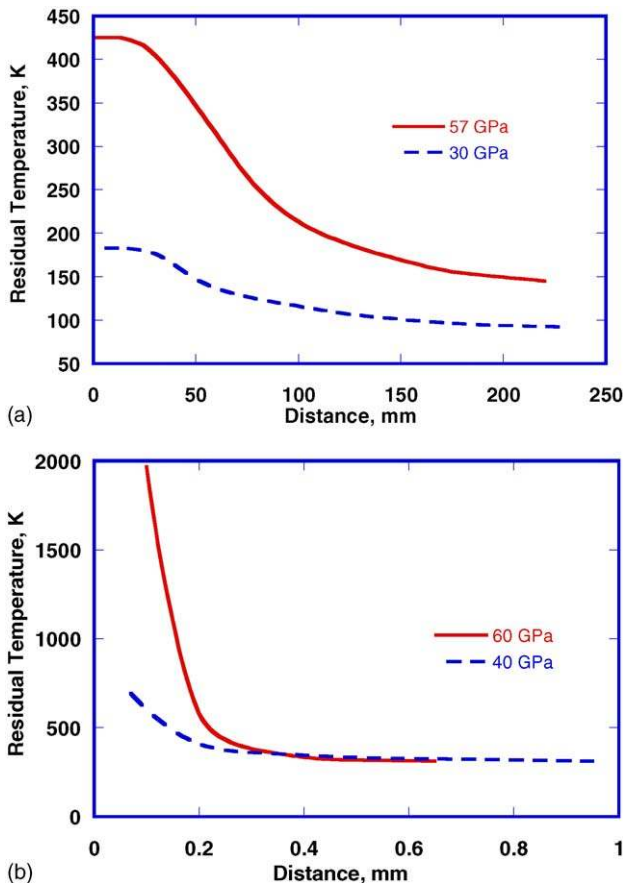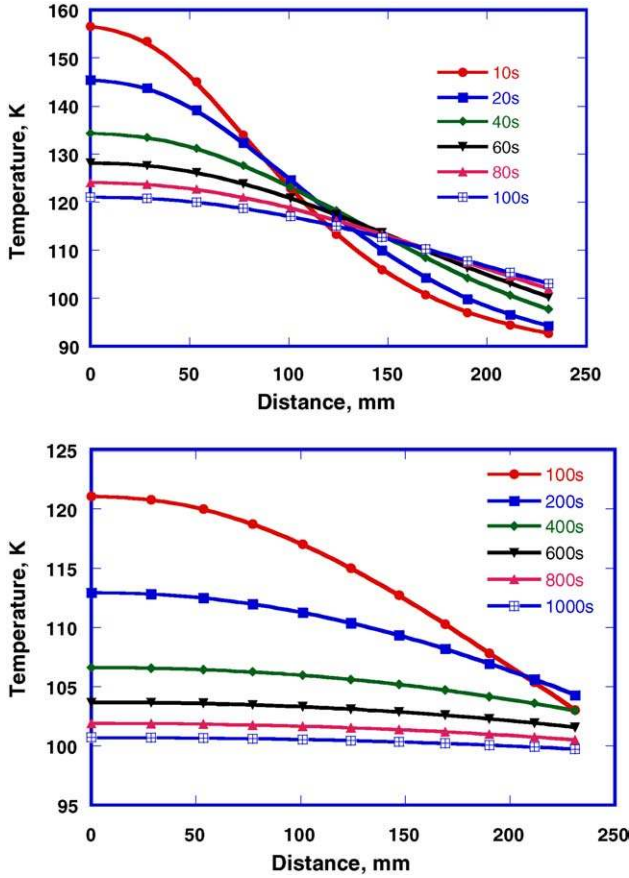
Fig. 12. Temperature change for copper plate-impacted at 30 GPa.
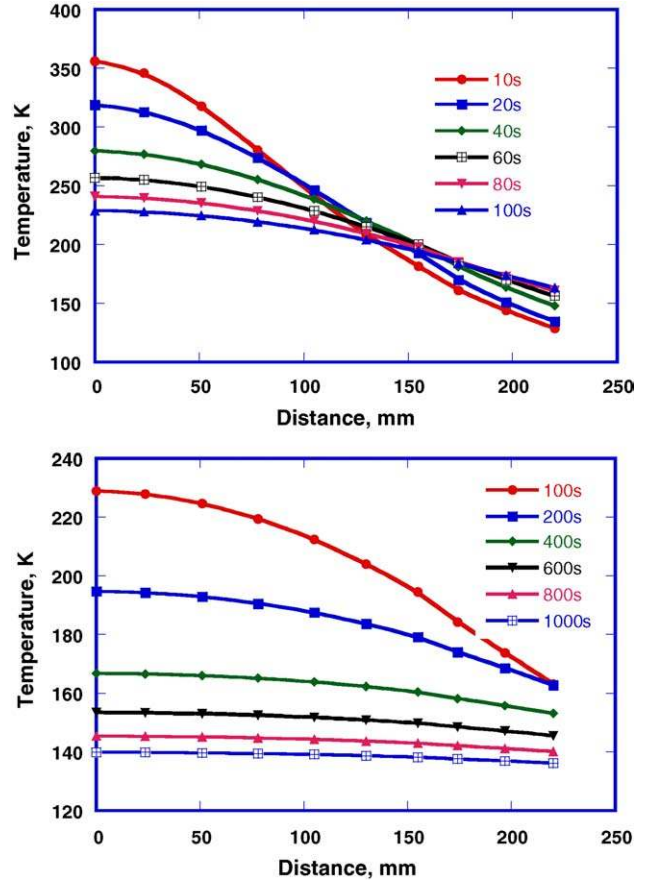

Fig. 13. Temperature change for copper plate-impacted at 57 GPa.

4.2. Heat generation in shear localization regions

Fig. 6(a) shows a shear localization area. Other observations also confirm the presence of localized regions of concentrated shear. The plastic deformation in these regions substantially exceeds those predicted from uniaxial strain, and one can expect local fluctuations in temperature. Indeed, the temperature rise in the shear localization areas can be calculated from the constitutive response of copper. This deformation-induced temperature rise was considered earlier by Lassila et al. [25]. It is expressed as:

$$\Delta T_{\mathrm{d}} = \frac{\beta}{\rho C_{\mathrm{p}}} \int_{\varepsilon_0}^{\varepsilon_1} \sigma \, \mathrm{d}\varepsilon \tag{16}$$

where ρ is the density, C_{p} the heat capacity, and β is the Taylor factor. For most metals, β is usually taken as 0.9–1.0. The strength of the material σ has to be estimated under specified conditions in different cases. We use the Johnson–Cook [38] equation:

$$\sigma = (\sigma_0 + B\varepsilon^n) \left(1 + C \log \frac{\dot{\varepsilon}}{\varepsilon_0}\right) [1 - T^{*m}] \tag{17}$$

where

$$T^* = \frac{T - T_{\mathrm{r}}}{T_m - T_{\mathrm{r}}} \tag{18}$$

The temperature change due to the plastic deformation is expressed as:

$$T^* = 1 - \exp \left[\frac{-0.9 \left(1 + C \log \frac{\dot{\varepsilon}}{\dot{\varepsilon}_0}\right)}{\rho C_{\mathrm{p}}(T_m - T_{\mathrm{r}})} \times \left(\sigma_0 \varepsilon + \frac{B\varepsilon^{n+1}}{n+1}\right)\right] \tag{19}$$
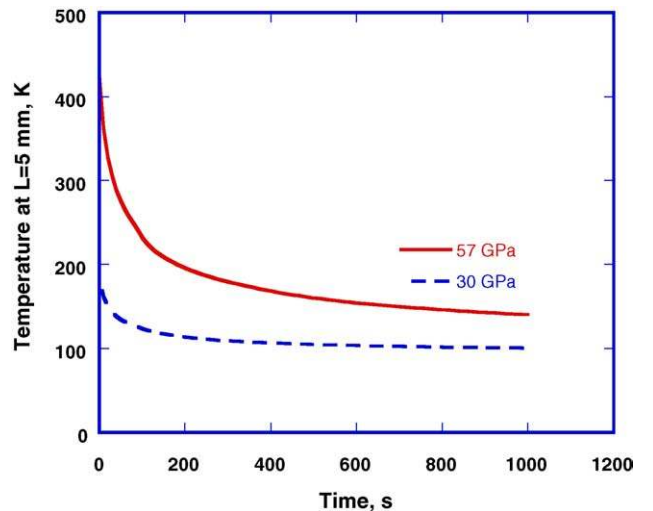

Fig. 14. Temperature change for fixed section at $L = 5$ mm along the plate-impacted sample.
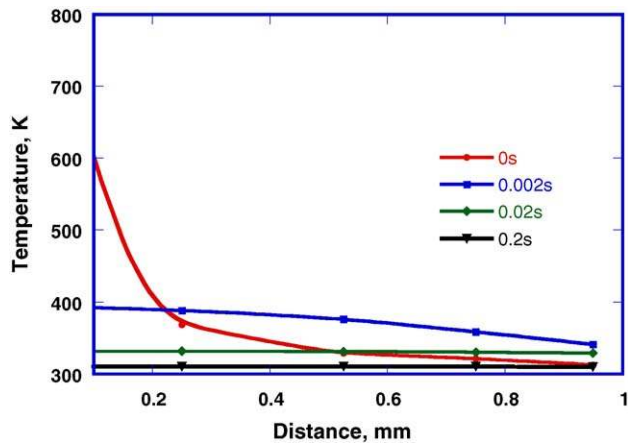
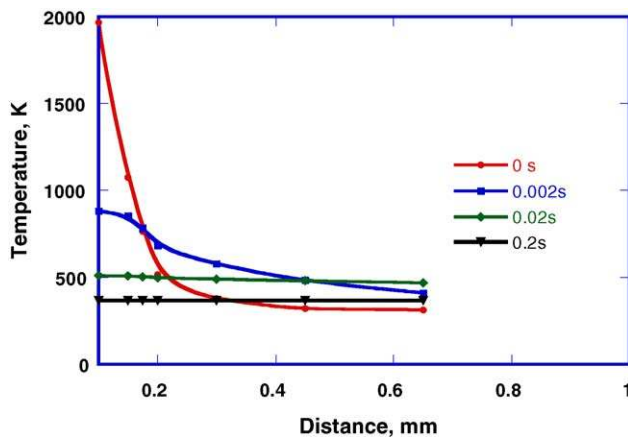Fig. 15. Temperature change in laser shocked copper with 200 J (40 GPa).

Fig. 16. Temperature change in laser shocked copper with 300 J (60 GPa).

where $T_r = 90$ K, $T_m = 1356$ K, $B = 53.7$ MPa, $C = 0.026$, $\sigma_0 = 330$ MPa (the value for shock hardened copper), $n = 0.56$, $m = 1.04$, $\rho_{90\,K} = 9.05$ g/cm^3, $C_{p,90\,K} = 260$ J/(kg K). Fig. 17 expresses the increase in temperature as a function of strain for a hypothetical shock hardened copper specimen. There is considerable local heat generation around heavily deformed
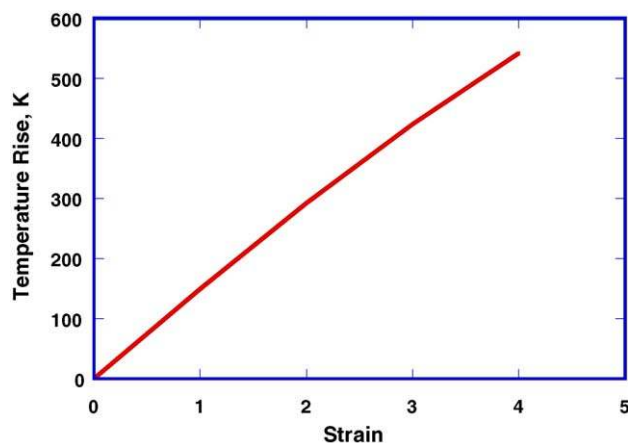

Fig. 17. Temperature rise due to plastic deformation.

areas (such as deformation bands). These regions can act as initiation sites for post-shock recrystallization.

5. Conclusions

Laser and plate-impact shocked copper with two orientations ([0 0 1] and [2 2 1]) revealed similarities as well as differences, that are interpreted in terms of the shock compression and thermal excursion processes. The observations can be summarized as:

- At lower pressures (30–40 GPa range), there are profuse stacking faults in the ⟨1 0 0⟩ orientation which have traces at 90° for both the laser and plate-impact experiments. The stacking-fault spacing is about the same 200–300 nm.
- In the 55–60 GPa range, micro-twins are observed for both the laser and plate-impact shocked ⟨1 0 0⟩ orientation.
- For the 57 GPa shock in both the ⟨1 0 0⟩ and ⟨2 2 1⟩ orientations, there are recrystallized grains for the plate impact case, while no recrystallized grains appeared in laser shocked samples.
- Regions of shear localization were observed after the plate impact shock, while they are absent after the laser shock. These micro-shear-bands have a thickness of approximately 1.5 μm.

The cooling times are calculated for the laser and plate-impact experiments. Plate-impact experiments were carried out at an initial temperature of 88 K whereas the laser shock experiments were conducted at ambient temperature. Nevertheless, the differences are of a factor of 5000. The differences in residual microstructures are attributed to the much larger cooling times in the plate-impact experiments. One possible explanation for the extensive recrystallization observed is the formation of shear concentration regions (shear bands) which can raise the local temperature by hundreds of degrees Centigrade (depending on the plastic strain), creating localized conditions for recrystallization.

References

[1] J.C.M. Li, in: L.E. Murr, C. Stein (Eds.), Frontiers in Materials Science—Distinguished Lectures, Marcel Dekker, New York, 1976, p. 527.
[2] J.C.M. Li, Metallic Glass, ASM, Metals Park, Ohio, 1976, pp. 224–246.
[3] J.C.M. Li, Proceedings of Fourth International Conference Rapidly Quenched Metals, Sendi, Japan, 1981.
[4] J.C.M. Li, Proc. Mater. Res. Soc. Symp. Rapidly Solidified Amorphous and Crystalline Alloys, Boston, 1981.

[5] J.C.M. Li, Trans. TMS-AIME 227 (1963) 75.

[6] J.C.M. Li, Can. J. Phys. 45 (1967) 493–509.

[7] I. Gupta, J.C.M. Li, Met. Trans. 1 (1970) 2323–2330.

[8] P. Zhu, J.C.M. Li, C.T. Liu, Reaction mechanism of combustion synthesis of NiAl, Mater. Sci. Eng. A 329 (2002) 57–68.

[9] J.C.M. Li, in: A.R. Rosenfield, G.T. Hahn, A.L. Bement, R.I. Jaffee (Eds.), Dislocation Dynamics, McGraw-Hill, New York, 1968, pp. 87–116.

[10] C.S. Smith, Trans. AIME 212 (1958) 574.

[11] P.S. Decarli, M.A. Meyers, in: M.A. Meyers, L.E. Murr (Eds.), Shock Waves and High-Strain-Rate Phenomena in Metals, 1981, pp. 341–373.

[12] P.C. Chou, J. Carleone, J. Appl. Phys. 48 (1977) 4187–4195.

[13] J.M. Walsh, J. Appl. Phys. 56 (1984) 1997–2006.

[14] D.E. Grady, J. Impact Eng. 5 (1987) 285–293.

[15] C.Y. Hsu, K.C. Hsu, L.E. Murr, M.A. Meyers, in: M.A. Meyers, L.E. Murr (Eds.), Shock Waves and High-Strain-Rate Phenomena in Metals, 1981, pp. 433–452.

[16] G.T. Gray III, Mater. Res. Soc. Symp. Proc. 499 (1998) 87–98.

[17] M.A. Meyers, Dynamic Behavior of Materials, John Wiley and Sons Inc., New York, 1994.

[18] K.S. Vecchio, U. Andrade, M.A. Meyers, L.W. Meyer, Shock Compression of Condensed Matter, 1991, pp. 527–530.

[19] B.A. Remington, G. Bazan, J. Belak, E. Bringa, M. Caturla, J.D. Colvin, M.J. Edwards, S.G. Glendinning, D.S. Ivanov, B. Kad, D.H. Kalantar, M. Kumar, B.F. Lasinski, K.T. Lorenz, J.M. Mcnaney, D.D. Meyerhofer, M.A. Meyers, S.M. Pollaine, D. Rowley, M. Schneider, J.S. Stölken, J.S. Wark, S.V. Weber, W.G. Wolfer, B. Yaakobi, L.V. Zhigilei, Metall. Mater. Trans. 35A (2004) 2587–2607.

[20] G.T. Gray III, E.S. Follansbee, C.E. Frantz, Mater. Sci. Eng., A 111 (1989) 9–16.

[21] M.A. Mogilevsky, L.A. Teplyakova, in: L.E. Murr, K.P. Staudhammer, M.A. Meyers (Eds.), Metallurgical Applications of Shock-Wave and High-Strain-Rate Phenomena, Marcel Dekker, New York, 1986, pp. 419–427.

[22] M. Pollington, P. Thompson, J. Maw, Discov. Sci. Technol. J. AWE 5 (2002) 16–25.

[23] R. Cauble, T.S. Perry, D.R. Bach, K.S. Budil, B.A. Hammel, G.W. Collins, D.M. Gold, J. Dunn, P. Celliers, Phys. Rev. Lett. 80 (1998) 1248–1251.

[24] J.F. Ready, Industrial Applications of Lasers, Academic Press, San Diego, 1997.

[25] D.H. Lassila, T. Shen, B.Y. Cao, M.A. Meyers, Metall. Mater. Trans. 35A (2004) 2729–2739.

[26] M.A. Meyers, F. Gregori, B.K. Kad, M.S. Schneider, D.H. Kalantar, B.A. Remington, G. Ravichandran, T. Boehly, J.S. Wark, Acta. Metall. 51 (2003) 1211–1228.

[27] J. Lindl, Phys. Plasmas 2 (1995) 3933–3982.

[28] L.E. Murr, K.P. Staudhammer, Mater. Sci. Eng. 20 (1975) 35–46.

[29] L.E. Murr, Scripta Met. 12 (1978) 201–206.

[30] L.E. Murr, in: M.A. Meyers, L.E. Murr (Eds.), Shock Waves and High-Strain-Rate Phenomena in Metals, Plenum, NY, 1981, pp. 607–673.

[31] J.C. Huang, G.T. Gray III, Acta Metall. 37 (12) (1989) 3335–3347.

[32] H. Mughrabi, T. Ungár, W. Kienle, M. Wilkens, Philos. Mag. A 53 (1986) 793–813.

[33] O. Johari, G. Thomas, Acta. Metall. 12 (1964) 1153–1159.

[34] G.T. Gray III, P.S. Follansbee, in: C.Y. Chiem, H.D. Kunze, L.W. Meyers (Eds.), Impact Loading and Dynamic Behavior of Materials, Informationsgells, Verlag, 1988, p. 541.

[35] G.T. Gray III, in: M.A. Meyers, L.E. Murr, K.P. Staudhammer (Eds.), Shock-Wave and High-Strain-Rate Phenomena in Materials, Dekker, NY, 1992, pp. 899–911.

[36] R. Zauter, F. Petry, M. Bayerlein, C. Sommer, H.-J. Christ, H. Mughrabi, Philos. Mag. A 66 (1992) 425–436.

[37] F. Kreith, M.S. Bohn, Principles of Heat Transfer, Brooks/Cole, CA, 2000.

[38] G.R. Johnson, W.H. Cook, Proceedings of Seventh International Symposium on Ballistics ADPA, the Netherlands, 1983.